URSI GASS 2020, Rome, Italy, 29 August - 5 September 2020

Preliminary Study on the Feasibility of Reconstructing Anatomically Complex Numerical Brain Phantoms with Limited Prior Information

Pan Lu, Syed Ahsan, and Panagiotis Kosmas
Department of Engineering, King's College London, London, UK

Abstract

In this paper, we present a preliminary study of brain imaging by using MWI algorithms when limited prior information is given. By using the distorted Born iterative method with the fast iterative shrinkage thresholding algorithm, reconstructions are performed for different kinds of head models based on the anatomically complex numerical Zubal head phantom. Results show that the quality of the reconstructed images decreases when less prior information is given.

1 Introduction

Microwave imaging (MWI) is gaining increasing interest worldwide, and it has the potential to be designed as a low-cost and portable device, which can become an alternative imaging technique for early-stage diagnostics [1, 2]. One possible application of MWI is brain imaging for stroke detection [3].

MWI methods reconstruct the distribution of dielectric properties of tissues by solving an electromagnetic (EM) inverse scattering problem [4], which relies on the contrast between the normal and malignant tissues due to water content [1]. In this paper, the distorted Born iterative method (DBIM) [5] with fast iterative shrinkage thresholding algorithm (FISTA) [6] is used as the imaging algorithm in terms of its robustness and efficiency, which is proposed by our recent work [7].

The interaction of microwaves with the head is highly nonlinear due to the complex structure of the head and brain. This results in a challenging EM inverse scattering problem with reconstruction accuracy that depends heavily on the available prior information. As this information is difficult or impractical to obtain, it is important to look at what can be achieved using different imaging scenarios. The aim of this paper is to examine this problem by using the MRI-derived Zubal head phantom [8] to create different scenarios and benchmark imaging performance in ideal simulation conditions.

The remainder of this paper is organized as follows: In Section 2, we review the formulation of the DBIM for MWI problems with FISTA as the linear solver. Reconstruction results of different kinds of head models based on the Zubal head phantom are presented in Section 3, followed by conclusions in Section 4.

2 Methods

The DBIM is an iterative method for solving inverse scattering problems based on the Born approximation, which is used to estimate the spatial distribution of dielectric properties inside a region V [4]. For each transmitter-receiver (TR) pair, the DBIM integral equation where the total field is replaced by the background field is organized as follows,

$$\begin{aligned} E_s(\boldsymbol{r_n}, \boldsymbol{r_m}) &= E_t(\boldsymbol{r_n}, \boldsymbol{r_m}) - E_b(\boldsymbol{r_n}, \boldsymbol{r_m}) \\ &= \omega^2 \mu_0 \varepsilon_0 \int_V G_b(\boldsymbol{r_n}, \boldsymbol{r}) E_b(\boldsymbol{r}, \boldsymbol{r_m}) \delta_\varepsilon(\boldsymbol{r}) d\boldsymbol{r}, \end{aligned} \tag{1}$$

where E_t, E_s, E_b are the total, scattered and background fields respectively, $\boldsymbol{r_n}$ and $\boldsymbol{r_m}$ are the transmitting and receiving antenna locations, ω is the angular frequency, μ_0 is the relative permeability, ε_0 is the relative permittivity, and G_b is the Green's function for the background medium. The contrast δ_ε between the relative complex permittivities of the reconstruction domain $\varepsilon(\boldsymbol{r})$ and background $\varepsilon_b(\boldsymbol{r})$ is defined as $\delta_\varepsilon(\boldsymbol{r}) = \varepsilon_r(\boldsymbol{r}) - \varepsilon_b(\boldsymbol{r})$.

By discretizing all the TR pairs, the integral equation (1) leads to an under-determined and ill-conditioned linear system as,

$$\mathbf{A}\delta_\varepsilon = \mathbf{b} \tag{2}$$

where A is an $M \times N$ matrix ($M \ll N$), with M transmit-receive pairs and N voxels of the reconstruction region V, b is a $M \times 1$ vector of the scattered fields.

The background fields at each DBIM iteration i is calculated by the forward solver, and then the linear system (2) is constructed by DBIM, which is solved by the inverse solver. At each iteration i, the background permittivity is updated by $\varepsilon_b^{i+1}(\boldsymbol{r}) = \varepsilon_b^i(\boldsymbol{r}) + \delta_\varepsilon(\boldsymbol{r})$.

In this paper, the finite difference time domain (FDTD) method is used as the forward solver and the FISTA is used as the inverse solver [7]. The single-pole Debye model is

employed for FDTD to model the frequency-dependent materials as,

$$\varepsilon_r(\omega) = \varepsilon_\infty + \frac{\Delta\varepsilon}{1+j\omega\tau} + \frac{\sigma_s}{j\omega\varepsilon_0}, \tag{3}$$

where ε_∞, $\Delta\varepsilon$, τ and σ_s are the parameters of the Debye model. To solve the ill-conditioned linear system, a minimization problem with a regularization term is considered by FISTA as [6],

$$F(\mathbf{x}) = \frac{1}{2}\|\mathbf{A}\mathbf{x}-\mathbf{b}\|_2^2 + \lambda\|\mathbf{x}\|_p \tag{4}$$

where λ is a regularization parameter, $\|\cdot\|_p = \sqrt[p]{|\cdot|^p}$, and usually the l_1-norm is chosen. Thus the structure of FISTA is constructed as [6],

$$\begin{aligned} \mathbf{x}_k &= p_L(\mathbf{y}_k), \\ t_{k+1} &= \frac{1+\sqrt{1+4t_k^2}}{2}, \\ \mathbf{y}_{k+1} &= \mathbf{x}_k + \frac{t_k-1}{t_{k+1}}(\mathbf{x}_k - \mathbf{x}_{k-1}) \end{aligned} \tag{5}$$

where $t_0 = 1$, p_L is the soft thresholding function, and $\mathbf{y_k}$ is the solution at the k–th iteration.

3 Results

In this section, the MRI-derived Zubal head phantom [8] is used for the reconstructions, which is 256 × 256 × 128 voxels with size of 1.1 mm × 1.1 mm × 1.4 mm. As we only consider 2D reconstructions in this paper, a slice of the Zubal head phantom is used as shown in Fig. 1. The

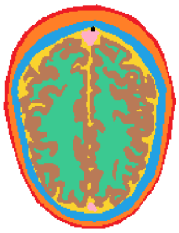

Figure 1. Selected 2D slice of the Zubal head phantom.

original slice has 8 materials, including skin marked in red, fat marked in orange, bone marked in blue, cerebrospinal fluid (CSF) marked in yellow, blood marked in black, dura marked in pink, gray matter marked in brown and white matter marked in green, from the outer to the inner.

Based on this slice, several models are created in FDTD with each voxel of size 2 mm × 2 mm, which are used for reconstruction. These models are immersed in a homogeneous background filled with 90% glycerol water mixture with $\varepsilon_\infty = 6.566$, $\Delta\varepsilon = 16.86$ and $\sigma_s = 0.3231$, which is used in our recent experiment work [9]. The relaxation time τ is fixed as 0.14288 ns for all the materials. The total size of these models is 125 × 125 (250 mm × 250 mm). The Debye parameters of these materials are obtained by curve fitting the permittivy values from the IT'IS database [10], shown in Table. 1. A modulated Gaussian pulse is employed as the source excitation for FDTD as,

$$g(t) = sin(2\pi ft)e^{-\frac{(t-t_0)^2}{t_d^2}}, \tag{6}$$

with a central modulation frequency f set at 1.0 GHz, a time delay t_0=1.08ns, and a pulse duration t_d=0.32ns. For all the reconstructions, 40 DBIM iterations are performed.

Table 1. Debye parameters for the Zubal head phantom.

Tissue type(and color in Fig. 1)	ε_∞	$\Delta\varepsilon$	σ_s
skin(red)	37.65	11.36	0.6241
fat(orange)	8.609	2.922	0.07526
bone(blue)	8.483	4.381	0.08252
white matter(green)	35.89	6.729	0.4476
gray matter(brown)	40.03	14.47	0.7158
blood(black)	44.67	18.02	1.322
CSF(yellow)	66.08	4.606	2.338
dura(pink)	39.89	6	0.8537

The first model is the full head and a blood target with radius 15 mm, shown in Fig. 2(a), where eight antennas are placed in a circle with radius 100 mm, marked in white color. Assuming that the full head is known except the blood target in Fig. 2(b), the reconstruction results of ε_∞ at 1 GHz are shown in Fig. 2(c) and Fig. 2(d) where the color bar is changed to show the results better.

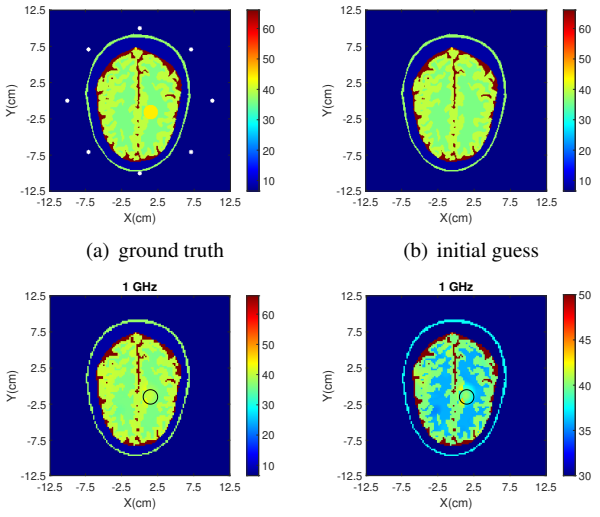

(a) ground truth (b) initial guess

(c) reconstruction (d) reconstruction

Figure 2. Reconstruction results of ε_∞ of the full head plus the blood target at 1 GHz: (a) ground truth, (b) initial guess, (c) reconstruction, (d) reconstruction with changed color bar.

As the area of the gray matter is large, it is not easy to reconstruct the whole model with such a complicated config-

uration with zero knowledge. Thus we have also examined a simplified model which changes the gray matter to white matter, shown in Fig. 3(a). When only the boundary of the head is given as Fig. 3(b), the initial start for the reconstruction corresponds to the homogeneous white matter. To deal with the increased non-linearity, 16 antennas placed in an ellipse with long axis 100 mm and short axis 85 mm are used to collect more information. As can be seen from the reconstruction results in Figs 3(c) and 3(d), both the blood target and the boundary of the brain are reconstructed.

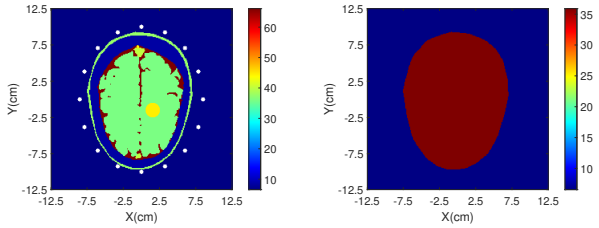

(a) ground truth (b) initial guess

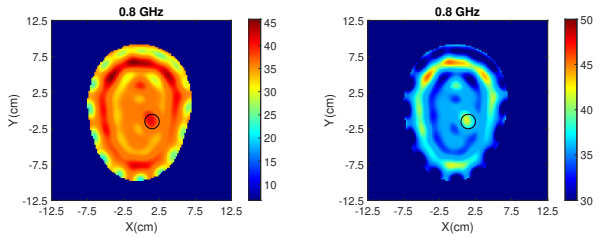

(c) reconstruction (d) reconstruction

Figure 3. Reconstruction results of ε_∞ of the head without gray matter at 0.8 GHz: (a) ground truth, (b) initial guess, (c) reconstruction, (d) reconstruction with changed color bar.

As replacing gray matter with white is not realistic and only served as a benchmark test, we also examined if a simplified model of the head which includes both white and gray matter can be reconstructed. To this end, we used a three-layer phantom (skin, white matter, and gray matter) and two different models as initial guess, shown in Figs 4 and 5. For all the following reconstructions, 16 antennas placed in an ellipse are used, same as before. The original ε_∞ of this model is shown in Fig. 4(a). The first reconstruction is performed when the skin layer is known and the inner brain is set as white matter, with the initial guess shown in Fig. 4(b). The gray matter is successfully reconstructed as shown in Figs 4(c) and 4(d).

Moreover, a second reconstruction of the same model in Fig. 4(a) has been performed, but with less prior information, the same as in Fig. 3(b) where only the boundary of the head is known. The reconstruction results are shown in Fig. 5. The gray matter is again reconstructed but with lower accuracy, which is anticipated due to loss in prior information in the initial guess.

In our tests, reconstructions are performed at different frequencies, and the reconstruction results at adjacent frequencies not shown in this paper also show similar images. In addition to the results presented in the paper, we have studied further the problem of reconstructing models of multiple layers (beyond the simplified model of Fig. 4(a)) with limited prior information, and we will present representative results in the conference. In summary, when only the boundary of the head is known, the results are not convincing due to the non-linearity of the problem. A possible approach to improve reconstruction quality is to break down the reconstruction process to two steps, with the first aiming to reconstruct a more accurate initial guess that can enable a more accurate reconstruction in the second step.

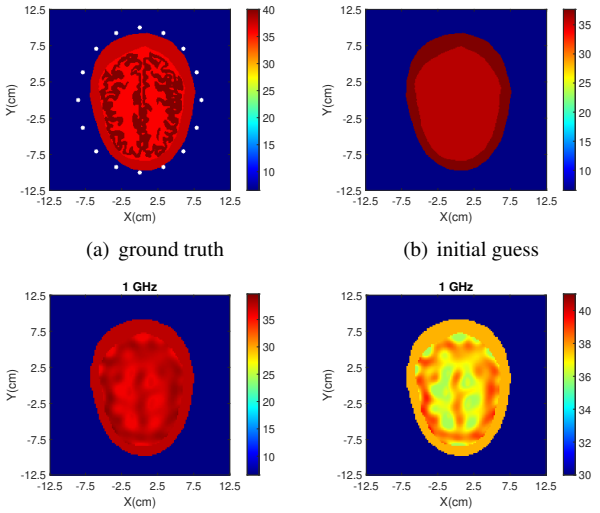

(a) ground truth (b) initial guess

(c) reconstruction (d) reconstruction

Figure 4. Reconstruction results of ε_∞ of the three-layer head at 1 GHz: (a) ground truth, (b) initial guess, (c) reconstruction, (d) reconstruction with changed color bar.

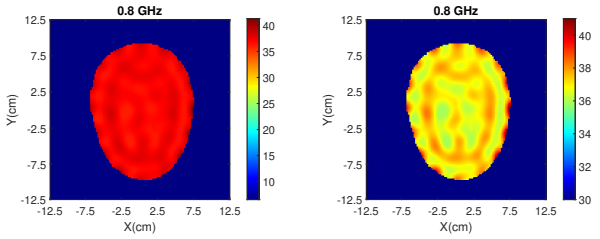

(a) reconstruction (b) reconstruction

Figure 5. Reconstruction results of ε_∞ of the three-layer head at 0.8 GHz: (a) reconstruction, (b) reconstruction with changed color bar.

4 Conclusions

We have presented the reconstructions results of several head models with different layers based on the Zubal head phantom by using the DBIM-FISTA method. As the complexity of the head phantom increases, more information is required to be collected by the antennas and more prior information are needed to improve the reconstructed images

of the dielectric properties. More reconstruction results will be presented at the conference.

5 Acknowledgements

This research was funded in part by Innovate UK grant number 103920 and in part by the Engineering and Physical Sciences Research Council grant number EP/R013918/1.

References

[1] S. Semenov, "Microwave tomography: review of the progress towards clinical applications," *Philosophical Transactions of the Royal Society A: Mathematical, Physical and Engineering Sciences*, vol. 367, no. 1900, pp. 3021–3042, 2009.

[2] P. Kosmas and L. Crocco, "Introduction to special issue on "Electromagnetic technologies for medical diagnostics: Fundamental issues, clinical applications and perspectives," *Diagnostics*, vol. 9, no. 1, p. 19, 2019.

[3] M. Hopfer, R. Planas, A. Hamidipour, T. Henriksson, and S. Semenov, "Electromagnetic tomography for detection, differentiation, and monitoring of brain stroke: A virtual data and human head phantom study." *IEEE Antennas and Propagation Magazine*, vol. 59, no. 5, pp. 86–97, 2017.

[4] D. W. Winters, J. D. Shea, P. Kosmas, B. D. Van Veen, and S. C. Hagness, "Three-dimensional microwave breast imaging: Dispersive dielectric properties estimation using patient-specific basis functions," *IEEE Transactions on Medical Imaging*, vol. 28, no. 7, pp. 969–981, July 2009.

[5] W. C. Chew and Y. M. Wang, "Reconstruction of two-dimensional permittivity distribution using the distorted Born iterative method," *IEEE Transactions on Medical Imaging*, vol. 9, no. 2, pp. 218–225, June 1990.

[6] A. Beck and M. Teboulle, "A fast iterative shrinkage-thresholding algorithm for linear inverse problems," *SIAM Journal on Imaging Sciences*, vol. 2, no. 1, pp. 183–202, 2009. [Online]. Available: https://doi.org/10.1137/080716542

[7] P. Lu, J. Córcoles, and P. Kosmas, "Non-linear microwave imaging using fast iterative shrinkage thresholding," in *2019 Progress in Electromagnetics Research Symposium (PIERS-Rome)*, June 2019.

[8] I. G. Zubal, C. R. Harrell, E. O. Smith, Z. Rattner, G. Gindi, and P. B. Hoffer, "Computerized three-dimensional segmented human anatomy," *Medical physics*, vol. 21, no. 2, pp. 299–302, 1994.

[9] S. Ahsan, Z. Guo, Z. Miao, I. Sotiriou, M. Koutsoupidou, E. Kallos, G. Palikaras, and P. Kosmas, "Design and experimental validation of a multiple-frequency microwave tomography system employing the DBIM-TwIST algorithm," *Sensors*, vol. 18, no. 10, p. 3491, 2018.

[10] P. Hasgall, E. Neufeld, M. Gosselin, A. Klingenböck, N. Kuster, P. Hasgall, and M. Gosselin, "It'is database for thermal and electromagnetic parameters of biological tissues," 2012.